Hif-1α stabilisation polarises macrophages via cyclooxygenase/prostaglandin E2 *in vivo*

[1,2]Amy Lewis and [1,2]Philip M. Elks

[1]The Bateson Centre, University of Sheffield, Western Bank, Sheffield, UK. [2]Department of Infection and Immunity and Cardiovascular Disease, University of Sheffield, Western Bank, Sheffield, UK.

Corresponding author:
Dr Philip M. Elks
The Bateson Centre,
University of Sheffield,
Firth Court,
Western Bank,
Sheffield,
South Yorkshire,
S10 2TN.
UK
Tel: +44 (0) 1142 223609
p.elks@sheffield.ac.uk

Abstract

Macrophage subtypes are poorly characterised in disease systems *in vivo*. The initial innate immune response to injury and infectious stimuli through M1 polarisation is important for the outcome of disease. Appropriate macrophage polarisation requires complex coordination of local microenvironmental cues and cytokine signalling to influence immune cell phenotypes. If the molecular mechanisms behind macrophage polarisation were better understood then macrophages could be pharmacologically tuned to better deal with bacterial infections, for example tuberculosis. Here, using zebrafish *tnfa:GFP* transgenic lines as *in vivo* readouts of M1 macrophages, we show that hypoxia and stabilisation of Hif-1α polarises macrophages to a *tnfa* expressing phenotype. We demonstrate a novel mechanism of Hif-1α mediated macrophage *tnfa* upregulation via a cyclooxygenase/prostaglandin E2 axis, a mechanism that is conserved in human primary macrophages. These findings uncover a novel macrophage HIF/COX/TNF axis that links microenvironmental cues to macrophage phenotype that may have implications in inflammation, infection and cancer, where hypoxia is a common microenvironmental feature and where cyclooxygenase and Tnfa are major mechanistic players.

Introduction

The innate immune response to injury and pathogen invasion are complex and are tightly regulated by coordination of microenvironmental cues and cytokine signalling. Macrophages are important innate immune cells in disease and their activation states, commonly termed polarisation states, are especially important during the early response to injury and infection. Mammalian macrophages have been classified into two broad polarisation/activation states; M1 (or classically activated) and M2 (alternatively activated) (1). Pro-inflammatory, or M1, macrophages are highly antimicrobial and can phagocytose and efficiently kill bacteria. Macrophages are also central players in tissue healing and restoration of homeostasis post injury/infection, which requires a change in macrophage

phenotype to a wound healing, M2, state (2). A diverse variety in macrophage function has been observed in many *in vitro* systems, yet control of macrophage subsets remains poorly understood *in vivo*. Current classifications are based on *in vitro* mammalian datasets, using monocytes that have been polarised to different macrophage phenotypes by addition of cytokine-cocktails to the media (3). Specific subsets of macrophage polarisation are context dependent *in vivo* and subtle changes in the microenvironment can lead to different phenotypes of M1 and M2 macrophages, reflecting a spectrum rather than a binary classification of behaviours (4). One important microenvironmental factor is hypoxia, which has profound effects on macrophage phenotypes (5). To fully understand how microenvironmental cues affect macrophage polarisation, *in vivo* systems are required to study macrophage behaviour over time and space without disturbance from extrinsic factors. Determining the molecular triggers and polarisation states of macrophages could open up possibilities to manipulate macrophage phenotype during disease as novel therapeutic avenues.

The tissue macrophage response to injury/bacterial infections is a rapid, pathogen recognition receptor (PPR) mediated, switch to an M1 type phenotype, characterised by production and release of pro-inflammatory mediators, including cytokines such as IL-1β, IL-6, IL-12 and TNF (6, 7). This phenotypic switch is required for a successful response to the invading pathogen and for clearance before infection can take hold (8, 9). However, in the case of intracellular pathogens, such as *Mycobacterium tuberculosis* (Mtb), this macrophage response is subverted, establishing a protective niche within innate immune cells (10–13). This bacterial-mediated interference in macrophage polarisation highlights a gap for potential therapeutic tuning of the macrophage response to allow for bacterial clearance (14, 15).

One potential macrophage tuning mechanism is via the Hypoxia Inducible Factor (HIF) -1α transcription factor (16). HIF-1α is a master transcriptional regulator of the cellular response to low levels of oxygen (hypoxia) (17). Leukocytes, including macrophages and

neutrophils, are exquisitely sensitive to tissue hypoxia, a signature of many disease microenvironments (eg infections and cancer) due to lack of local blood supply and a high turnover of local oxygen by pathogens (5, 18). Hypoxia and HIF-1α stabilisation have been shown to have activating effects on macrophages *in vitro*, increasing their M1 profile and bactericidal capabilities, yet the pro-inflammatory mechanisms behind this are not well understood *in vivo* (5).

Hypoxia is a microenvironmental signal that increases epithelial cyclooxygenase/prostaglandin E2 production in cancer models (19–21). Eicosanoids are lipid signalling molecules and important pro-inflammatory mediators which are produced, and released, by macrophages during early microbial infection (22, 23). The best characterised of these are prostaglandins, strong inflammatory mediators that are known to affect macrophage polarisation states during infection (24). A key family of enzymes for prostaglandin biosynthesis is the cyclooxygenases (COX). COX-1 and -2 enzymes are responsible for the production of prostaglandins as breakdown products of arachidonic acid. Prostaglandins, in turn, are highly immunomodulatory, synergising with cytokines to amplify pro-inflammatory responses (25). The potential effects of hypoxia-induced prostaglandins on macrophage polarisation have not been investigated *in vivo*. Recent evidence indicates that a HIF/COX/TNF axis may exist, with hypoxia-induced TNF expression in osteoblasts (bone producing cells) being mediated via cyclooxygenase enzymes by an, as yet, unknown mechanism (26). If observed in macrophages, this HIF/COX/TNF axis could have important pro-inflammatory outcomes in disease and represent a novel therapeutic avenue.

Zebrafish have emerged as a useful model to understand innate immune cells in their *in vivo* microenvironment (27). Development of multiple innate immune cell transgenic lines, combined with non-invasive fluorescence imaging, has enabled mechanistic investigation into macrophage biology (2, 28, 29). Well-characterised models of inflammation and infection biology have emerged using zebrafish larvae. Mechanistic insights into neutrophil and macrophage recruitment to an injury site have been gained through use of a tailfin transection model (30), while host-pathogen interactions have been studied using the

111 natural fish pathogen *Mycobacterium marinum* (Mm) as a model of tuberculosis (27).
112 Recently, it has been demonstrated that *tnfa* promoter driven fluorescent transgenic lines
113 display an M1 type phenotype upon sterile injury immune challenge (31, 32). This advance
114 has enabled us to investigate macrophage polarisation within the zebrafish system during a
115 host-pathogen immune challenge. We have previously demonstrated that Hif-1α stabilisation
116 induces macrophage proinflammatory *il-1β* transcription and that this is host-protective
117 against Mm infection in the zebrafish model (33). We therefore hypothesised that Hif-1α
118 stabilisation would promote macrophage pro-inflammatory *tnfa* expression, via a
119 cyclooxygenase dependent mechanism, that could also be beneficial to the host during
120 infection.

121 Here, we investigated the regulation of expression of the important M1 pro-
122 inflammatory cytokine *tnfa* by Hif-1α stabilisation *in vivo*. We demonstrate that genetic,
123 pharmacological and hypoxia-mediated Hif-1α stabilisation upregulated macrophage *tnfa* in
124 zebrafish. We show that *tnfa* transcription is upregulated in macrophages after injury and
125 Mm infection (both at early- and granuloma- stage infection). We identify that Hif-1α
126 activates macrophage *tnfa* via cyclooxygenase/prostaglandin E2, while injury/Mm driven *tnfa*
127 production does not require active cyclooxygenase. Importantly, this novel macrophage
128 HIF/COX/TNF axis is conserved in primary human macrophages. These findings have
129 important implications in inflammation, infection and cancer biology where macrophage
130 polarisation states are influenced by microenvironmental hypoxia.
131
132 **Materials and Methods**
133
134 **Zebrafish**
135 Zebrafish were raised and maintained on a 14:10-hour light/dark cycle at 28ºC,
136 according to standard protocols (34), in UK Home Office approved facilities at The Bateson
137 Centre aquaria at the University of Sheffield. Strains used were Nacre (wildtype),

TgBAC(tnfa:GFP)pd1028, *Tg(tnfa:eGFP-F)ump5Tg*, *Tg(mpeg1:mCherry-F)ump2Tg, Tg(mpeg1:mCherryCAAX)sh378, Tg(lyz:Ds-RED2)nz50 TgBAC(il-1β:eGFP)sh445* and *Tg(phd3:EGFP)i144* (31, 32, 35–37).

Tailfin injury

Inflammation was induced in zebrafish embryos by tail transection as previously described (38). Embryos were anaesthetised at 2 days post fertilisation (dpf) by immersion in 0.168mg/ml Tricaine, and transection of the tail was performed using a scalpel blade. Larvae were imaged by confocal microscopy at 16 hour post wound (hpw) on a Leica TCS-SPE confocal on an inverted Leica DMi8 base and imaged using 20x or 40x objective lenses.

Mycobacterium marinum

Mm infection experiments were performed using M. marinum M (ATCC #BAA-535), containing a psMT3-mCherry or psMT3 mCrimson vector (39). Injection inoculum was prepared from an overnight liquid culture in the log-phase of growth resuspended in 2% polyvinylpyrrolidone40 (PVP40) solution (CalBiochem) as previously described (40). 100 or 150 colony forming units (CFU) were injected into the caudal vein at 28-30hpf as previously described (41).

Confocal microscopy of transgenic larvae

1dpi and 4dpi transgenic zebrafish larvae infected with fluorescent Mm strains were mounted in 0.8-1% low melting point agarose (Sigma-Aldrich) and imaged on a Leica TCS-SPE confocal on an inverted Leica DMi8 base and imaged using 20x or 40x objective lenses.

For quantification purposes acquisition settings and area of imaging were kept the same across groups. Corrected total cell fluorescence was calculated for each cell using Image J as previously described (42, 43).

RNA injections

Embryos were injected with dominant *hif-1αb* (ZFIN: *hif1ab*) variant RNA at the one cell stage as previously described (44). *hif-1α* variants used were dominant active (DA) and dominant negative (DN) *hif-1α*. Phenol red (PR) (Sigma Aldrich) was used as a vehicle control.

Pathway inhibitors

Unless otherwise stated, embryos were treated from 4 hours pre-Mm infection to 24 hours post infection (hpi) by addition to the embryo water and DMSO was used as a negative solvent control. The pan hydroxylase inhibitor, DMOG (dimethyloxaloylglycine, Enzo Life Sciences), was used at a 100μM concentration by incubation in E3 embryo media as previously described (44). The selective PHD inhibitors JNJ-402041935 (Cayman Chemicals) and FG-4592 (Selleckchem) were used at 100μM and 5μM respectively (45, 46). The selective inhibitor of COX-1, SC-560 (Cayman Chemicals), was used at 30μM and the selective inhibitor of COX-2, NS-398 (Cayman Chemicals), was used at 15μM by incubation in E3 embryo media as previously described (47). The 15-LOX inhibitor PD146176 (Tocris) was microinjected (1nl of 40nM) at 1 hour post infection (hpi). The leukotriene B4 receptor 1 (BLTR1) inhibitor, U-75302 (Abcam), was used at 30mM by incubation in E3 embryo media as previously described (48) together with the BLTR2 inhibitor, LY255283 (Abcam), which was used at 1mM. Exogenous prostaglandin E2 (Cayman Chemicals) and 15-keto-prostaglandin E2 (Cayman Chemicals) were added by incubation in E3 at a concentration of 1μM (49).

Hypoxia

Embryos were incubated in 5% oxygen (with 5% carbon dioxide) in a hypoxia hood (Baker-Ruskinn Sci-tive UM-027) from 32hpi for 6 hours and were imaged at 2dpf. Embryos from the same clutch kept in incubated normoxic room air were used as controls (33).

Bacterial pixel count

Mm mCherry infected zebrafish larvae were imaged at 4dpi on an inverted Leica DMi8 with a 2.5x objective lens. Brightfield and fluorescent images were captured using a Hammamatsu OrcaV4 camera. Bacterial burden was assessed using dedicated pixel counting software as previously described (50).

Human cells

Peripheral blood mononuclear cells (PBMC) were isolated by Ficoll-Paque PLUS (GE Healthcare) density centrifugation of whole blood from healthy donors (National Research Ethics Service reference 07/Q2305/7). PBMC were seeded at $2x10^6$/ml in 24-well tissue culture plates in RMPI 1640 media (Gibco) containing 2mmol/L L-glutamine (Lonza) and 10% newborn calf serum (Gibco). Cells were cultured in 5% CO_2 at 37ºC and non-adherent cells were removed after 24 hours. Remaining adherent cells were cultured for 14 days, with twice weekly media exchange, in RPMI 1640 supplemented with 2mmol/L L-glutamine and 10% heat-inactivated fetal bovine serum (FBS) (PAN Biotech) (51).

For experiments RPMI 1640 + 25mM HEPES (Gibco) containing 2mmol/L L-glutamine and 10% heat-inactivated FBS and drugs were pre-equilibrated in normoxia or hypoxia (0.8% O_2, 5% CO_2, 70% humidity at 37ºC) for 24 hours prior to the experiment (52).

Cells were introduced to the hypoxic workstation (Baker-Ruskinn Sci-Tive UM-027) where culture media was removed and replaced with hypoxia-equilibrated media as detailed above. Cells were treated in duplicate or triplicate wells with 100µg/ml LPS (InvivoGen), DMSO (Sigma-Aldrich), or 15mM COX-2 inhibitor (NS398) (Cayman Chemical) and incubated for 18 hours. For normoxic controls, cells were treated identically within a class-2 tissue culture hood and transferred to a normoxic tissue-culture incubator.

Cell supernatants were collected following 18 hours incubation in normoxia or hypoxia and were frozen for subsequent analysis. Culture supernatants were assayed in duplicate or triplicate using a human TNF ELISA MAX (Biolegend). In samples where undiluted supernatants fell outside the standard curve, samples were re-run following 1:10 dilution in assay buffer.

Statistical analysis

All data were analysed (Prism 7.0, GraphPad Software) using unpaired, two-tailed t-tests for comparisons between two groups and one-way ANOVA (with Bonferonni post-test adjustment) for other data. P values shown are: *$P < .05$, **$P < .01$, and ***$P < .001$.

Results

***tnfa:GFP* expression is upregulated by injury, infection and Hif-1α stabilisation**

TNF is a central regulator of the M1 inflammatory response to inflammation and pathogen challenge. Here, we use two transgenic zebrafish lines that express GFP via a *tnfa* promoter region; *TgBAC(tnfa:GFP)pd1028* and *Tg(tnfa:eGFP-F)ump5Tg* (31, 32). The *TgBAC(tnfa:GFP)pd1028* was made using BAC (bacterial artificial chromosome) transgenesis and contains 50kb of promoter region (32). The *Tg(tnfa:eGFP-F)ump5Tg* line has a smaller promoter region (3.8kb) than the BAC line (31) and has previously been demonstrated to be upregulated in macrophages after tailfin injury in a zebrafish model (31). Here, we demonstrate that this injury induced upregulation of macrophage *tnfa:GFP* is also found in the BAC transgenic line (*TgBAC(tnfa:GFP)pd1028* crossed to *Tg(mpeg1:mCherryCAAX)sh378)* shown 16 hours post wound (hpw) (Figure 1A). TNF has been implicated in all stages of TB infection, however the cell types involved *in vivo* have been difficult to observe (53). We used the *tnfa* BAC promoter GFP line to establish the transcriptional regulation of *tnfa* during pre- and early- larval Mm granuloma formation stages. *tnfa:GFP* expression was induced in larvae following Mm infection before granuloma

onset (at 1 day post infection, dpi), and after granuloma formation (at 4dpi) (Figure 1B). *tnfa:GFP* expression was predominantly found in macrophages with internalised Mm, shown by co-localisation of fluorescence with *mpeg-1:mCherry* expressing macrophages and mCrimson expressing Mm (Figure 1C). Macrophage expression was confirmed using the other *tnfa* promoter driven line, (*Tg(tnfa:eGFP-F)ump5Tg*, crossed to *Tg(mpeg1:mCherry-F)ump2Tg*) (Figure S1). Our data demonstrate that injury and Mm induced *tnfa* expression occurs in macrophages as part of an early M1 response.

Hif-1α can be stabilised in zebrafish both genetically and pharmacologically using dominant active constructs and hydroxylase inhibitors respectively (29, 44). We tested whether Hif-1α promotes M1 polarisation using the *tnfa:GFP* BAC transgenic line as a readout of M1 macrophages (31, 32). Hif-1α was stabilised genetically in larvae using DA Hif-1α RNA (44), which resulted in upregulation of *tnfa:GFP* expression (Figure 1D-F) indicating a shift of macrophage phenotype towards an activated M1 response. Dominant negative (DN) Hif-1α caused no upregulation of *tnfa:GFP* expression (Figure 1E-F). To demonstrate that it was also possible to boost the Hif-1α M1 pro-inflammatory response pharmacologically, the hypoxia mimetic DMOG (dimethyloxaloylglycine, a pan-hydroxylase inhibitor that stabilises Hif-1α via inactivation of regulatory prolyl hydroxylase enzymes) was used to stabilise endogenous levels of Hif-1α (57). DMOG treatment upregulated expression of *tnfa*:*GFP* compared to DMSO solvent controls, phenocopying the DA-Hif-1α response (Figure 1G). Recently described hypoxia mimetics with reportedly greater prolyl hydroxylase selectively, JNJ-42041935 and FG4592, had similar effects to DMOG (Figure 1H and I) (33, 45, 46). During both homeostasis and disease physiology, Hif-1α stability is regulated by microenvironmental hypoxia. To simulate this we subjected the *tnfa:GFP* line to 5% oxygen for 6 hours at 32hpf and looked for GFP expression at 48hpf. This level of hypoxia was sufficient to switch on GFP expression in the *Tg(phd3:GFP)i144* hypoxia reporter zebrafish (Figure S2) (33). Six hours of 5% oxygen increased *tnfa:GFP* expression at 48hpf, compared to normoxic controls, to a similar level as that observed with genetic or

pharmacological Hif-1α stabilisation (Figure 1J). Together, these data indicate that *tnfa* expression is part of a pro-inflammatory M1 macrophage response to hypoxia and stabilised Hif-1α, a response that is targetable by pharmacological agents and has the potential to aid the host response to bacterial challenge.

Hif-1α dependent *tnfa:GFP* transcription requires cyclooxygenase

Eicosanoids are lipid signalling molecules produced by macrophages during early microbial infection as part of an M1 response (22, 23). We tested whether cyclooxygenase inhibition affected Hif-1α mediated *tnfa:GFP* production. At basal levels, *tnfa:GFP* was not altered by the Cox-1 inhibitor SC560 or the Cox-2 inhibitor NS398 compared to DMSO treated negative controls (Figure 2A-B). Strikingly, DA Hif-1α-induced *tnfa:GFP* expression was significantly abrogated to basal levels by both SC560 and NS398 (Figure 2A-B). We have previously shown that DA Hif-1α induces the expression of another important pro-inflammatory cytokine, *il-1β,* shown by an *il-1β:GFP* transgenic line (Figure S3A) (33). Cox-1 inhibition by SC560 did not abrogate Hif-1α induced *il-1β:GFP*, while Cox-2 inhibition with NS398 caused a small decrease that did not reach basal levels (Figure S3B-C). These data indicate that Hif-1α-induced *tnfa* expression is caused by a product of the cyclooxygenase arm of the arachidonic acid pathway via a novel macrophage HIF/COX/TNF axis (Figure 2C), while Hif-1α induced *il-1β* does not fully act via this pathway suggestive of complex regulation of M1 pro-inflammatory cytokines by Hif-1α stabilisation.

We next tested whether injury- and infection-induced *tnfa* are cyclooxygenase dependent processes. Macrophage *tnfa:GFP* expression induced after injury was not abrogated by cyclooxygenase inhibition using NS398 (Figure 2D-E). Similarly, cyclooxygenase inhibition using either SC560 or NS398 did not alter the expression of Mm-induced *tnfa:GFP* (Figure 2F-G). Our data indicate that macrophage *tnfa* expression can be driven by the presence of DAMPS (injury) or PAMPS (Mm) and that these are cyclooxygenase independent mechanisms (Figure 2H).

We have previously shown that Hif-1α stabilisation is host-protective in the zebrafish Mm model, an effect that is dependent on macrophage expression of proinflammatory *il-1β* (33). We therefore hypothesised that priming macrophages with increased *tnfa* via Hif-1α stabilisation may be protective against subsequent Mm infection. Neither genetic nor pharmacological Hif-1α stabilisation were additive to the *tnfa:GFP* expression caused by either injury or Mm infection (Figure 2C-F and S4A-D). To test whether DA Hif-1α priming of macrophage *tnfa* had an effect on the outcome of Mm infection, bacterial burden was quantified in DA Hif-1α-injected embryos with cyclooxygenase inhibition (having demonstrated that Hif-1α-induced *tnfa* requires cyclooxygenase activity in Figure 2A-C). Neither SC560 nor NS398 mediated inhibition of Hif-1α-induced *tnfa* expression diminished the host-protective effect of DA Hif-1α (Figure S5A-C) or DMOG treated larvae (Figure S5D-F). Taken together these data indicate that injury- and Mm- induced *tnfa* is not further increased by Hif-1α stabilisation and that cyclooxygenase mediated early priming of *tnfa* in macrophages is not required for the Hif-1α mediated reduction of bacterial burden.

Blocking cyclooxygenase independent arachidonic acid pathways does not abrogate Hif-1α upregulation of *tnfa:GFP*

To investigate whether the effect of the cyclooxygenase inhibitors on *tnfa* was specific to the prostaglandin path of the arachidonic acid pathway, we targeted the lipoxin and leukotriene producing arms using the 15-Lipoxygenase inhibitor PD146176 and leukotriene B4 receptor antagonists. The 15-Lipoxygenase inhibitor PD146176 did not block the *tnfa:GFP* induced by DA Hif-1α (Figure 3A-B). Furthermore, PD147176 increased *tnfa:GFP* expression on its own in the absence of infection, although not to the same extent as DA Hif-α (Figure 3A-B). PD146176 also did not affect *tnfa:GFP* expression after Mm infection (Figure 3A-B), nor did it block the protective effect of DA Hif-1α. Treatment with PD146176 was sufficient to decrease Mm burden, but not to the same extent as DA Hif-1α (Figure 3C). Leukotriene B4 inhibition, using the BLTR1/2 antagonists U75302 and

328 LY255283, did not increase *tnfa:GFP* levels and also did not block DA Hif-1α induced
329 *tnfa:GFP* (Figure 3D-E). These data indicate that blocking components of the lipoxygenase
330 dependent arms of the arachidonic acid pathway do not block the Hif-1α effect on *tnfa*
331 expression and do not replicate the effects observed by blocking the cyclooxygenase
332 dependent arm (Figure 3F).
333
334 **Hif-1α-induced *tnfa:GFP* requires active prostaglandin E2**
335 A key family of immune regulators downstream of arachidonic acid and cyclooxygenases are
336 prostaglandins. The best characterised of these as a regulator of macrophage function is
337 prostaglandin E2 (PGE2). We tested whether PGE2 was a mediator in the HIF/COX/TNF
338 pathway by addition of exogenous PGE2 to DA Hif-1α larvae. Exogenous PGE2 had no
339 effect on *tnfa:GFP* expression in the absence or presence of Mm infection (Figure 4A-D).
340 However, PGE2 was able to rescue the decrease in *tnfa:GFP* expression after Cox-1 (Figure
341 4A and C) or Cox-2 (Figure 4B and D) inhibition in the DA Hif-1α larvae. Furthermore,
342 addition of PGE2 alone led to a significant increase in the DA Hif-1α-induced *tnfa:GFP*
343 expression (Figure 4A-D). These rescuing effects were not observed by addition of
344 exogenous 15-keto prostaglandin E2, an immunologically inactive degradation product of
345 PGE2 (Figure 4E-F) (49, 58, 59). These data indicate that Hif-1α-induced *tnfa:GFP* requires
346 active prostaglandin E2 (Figure 4G).
347
348 **The HIF-COX-TNF axis is conserved in human macrophages**
349 To translate our findings from zebrafish to humans we tested whether HIF-1α
350 stabilisation in human macrophages induces TNF expression. We found that human
351 monocyte derived macrophages (hMDMs) produced higher levels of TNF protein in hypoxia
352 (0.8% oxygen) than those in normoxia, measured by an anti-human TNF ELISA (Figure 5A).
353 Furthermore, treatment with the COX-2 inhibitor, NS398, reduced this hypoxia-induced TNF
354 back to the equivalent levels found in normoxia (Figure 5A). This was replicated when HIF-

355 1α was stabilised in hHDMs using the hypoxia mimetic FG4592 (Figure 5B). These data
356 indicate that the HIF/COX/TNF axis is a conserved mechanism in human macrophages and
357 could be important in human disease.
358
359 **Discussion**
360 Control of macrophage function during homeostasis and infection are critical for
361 healthy tissues and must integrate changes in the local microenvironment with cytokine
362 signalling. Understanding of signalling pathways that link the microenvironment with
363 macrophage phenotypic outcomes will identify potential novel therapeutic avenues for
364 control of macrophages during disease. Currently, the mechanisms and molecular cues
365 leading to different macrophage phenotypes are not well-defined *in vivo*.
366 Here we show that a disease relevant microenvironmental cue, hypoxia signalling via
367 Hif-1α, upregulates macrophage *tnfa* expression in a cyclooxygenase dependent manner *in*
368 *vivo*. TNF regulation by hypoxia has been shown in a range of mammalian cells, and its
369 promoter region contains HIF responsive elements (HREs), resulting in some level of direct
370 regulation by HIF-1α (60–63). We observed an M1 pro-inflammatory *tnfa* response with
371 stabilised Hif-1α, demonstrating that hypoxia signalling alone can lead to a switch of
372 macrophage polarisation to an M1 phenotype, consistent with our previous observations
373 concerning *il-1β* activation (33). Not only could *tnfa* activation be achieved by genetic
374 stabilisation of Hif-1α, but also using hypoxia mimetics and physiological hypoxia. These
375 findings indicate that the Hif-1α pro-inflammatory switch is targetable by pharmaceuticals
376 and could be druggable during disease. Hypoxic regulation of TNF via COX has previously
377 been demonstrated in mammalian osteoblasts, however, little is known about this interaction
378 (26). Our data demonstrate that Hif-1α upregulation of macrophage *tnfa* is dependent on
379 cyclooxygenase and further shows that the mechanism is likely to be via the production of
380 PGE2. The degradation metabolite 15-keto-PGE2 did not rescue the loss of *tnfa* expression
381 after cyclooxygenase inhibition, consistent with previous reports that 15-keto-PGE2 is

382 unable to bind the prostaglandin E2 EP receptors, demonstrating a requirement for active
383 PGE2 (64).

384 Mycobacteria mediated macrophage polarisation is complex, with M1 and M2
385 phenotypes observed during pathogenesis, however, the mechanisms determining
386 macrophage phenotype are not fully characterised (56). The Mtb/Mm granuloma has been
387 widely studied in human, mice and zebrafish and is rich in pro-inflammatory cytokine
388 production (32, 33, 65–69). Here, we observed that an M1 pro-inflammatory *tnfa* response
389 was induced at pre-granuloma stages as well as during granuloma formation *in vivo*. A key
390 advantage of using fluorescent transgenic zebrafish lines, such as *tnfa:GFP*, is that they
391 enable identification of the cell type producing the transgene in an intact organism. This is
392 especially important when studying early innate immune cell interactions with pathogens, as
393 it eliminates the risk of activation during a sorting process. TNF is required for the control of
394 initial TB infection in mice and also of latent TB in humans (68, 70–73). Patients on anti-TNF
395 therapies for immune diseases such as Crohn's disease and rheumatoid arthritis, which
396 have proved effective treatments for these debilitating illnesses, have an associated
397 increased risk of TB reactivation and infectious disease (72, 74). In the zebrafish Mm model
398 it has been widely demonstrated that Tnfa is required for control of early infection, with
399 perturbation of Tnfa signalling leading to high infectious burdens (75). When Hif-1α driven
400 *tnfa* was downregulated by cyclooxygenase inhibition, there was no effect on the decrease
401 in bacterial burden resulting from stabilisation of Hif-1α. Furthermore, none of the
402 arachidonic acid pathway inhibitors used in our study had any effect on Tnfa production after
403 Mm infection. These findings are consistent with Mm induced macrophage Tnfa production
404 being independent of arachidonic acid, and is most likely TLR mediated as has been
405 reported elsewhere (43, 56). Our data indicate that there is no additional protective effect of
406 priming macrophages with increased levels of Tnfa before infection onset. Interestingly, this
407 is not the case for another important M1 cytokine, Il-1β, where Hif-1α stabilisation fails to
408 reduce bacterial burden if Il-1β is blocked early in infection, (33). Our findings indicate that

409 different M1 cytokines induced by Hif-1α stabilisation can have differential effects on the
410 outcome of infection, and highlight that, although TNF and IL-1β are often used as markers
411 of M1 polarisation, their roles in the pro-inflammatory macrophage are distinct.

412 Blocking cyclooxygenase independent arms of the arachidonic acid pathway did not
413 inhibit Hif-1α-induced macrophage *tnfa* transcription in the same way as blocking the
414 cyclooxygenase/PGE2 arm. Inhibition of the 15-lipoxygenase arm was sufficient to induce
415 macrophage *tnfa* transcription which was host protective and decreased Mm burden. These
416 findings indicate a potential shift towards the COX/TNF dependent axis when 15-
417 lipoxygenase is blocked and are consistent with previous observations suggesting that
418 inhibition of 15-Lipoxygenase can have immune activating effects (48).

419 Our data reveal a novel mechanism of TNF activation in macrophages via a Hif-1α/
420 cyclooxygenase/PGE2 axis. Importantly, this pathway is conserved in human macrophages,
421 meaning that it could be targetable for pharmaceutical intervention to promote macrophage
422 M1-type polarisation in human disease. Although the effect of the HIF/COX/TNF axis in early
423 Mm infection was negligible, this pathway is likely to have important roles in numerous
424 disease situations. Multiple disease pathologies have hypoxia as a features of the tissue
425 microenvironment, concurrent with macrophage influx. Hif-1α mediated M1 switching and
426 TNF activation may be pertinent in later TB infection situations where granulomas have
427 stabilised Hif-1α due to necrotic and hypoxic centres (76, 77). It is not only bacterial
428 infections such as TB that might be influenced by a HIF-1α mediated M1/TNF switch.
429 Hypoxia is a key hallmark of cancers with high levels of HIF-1α widely found in those that
430 produce large tumours where the centre is hypoxic (78). This is also true of
431 cyclooxygenase/PGE2 production, where these important immunomodulatory signals are
432 required for cellular adaption to the tumour microenvironment (79). Certain types of cancer
433 induce inflammatory microenvironments, where cytokines and other immunomodulators can
434 contribute to the progression of cancers (80). Macrophages play central roles in cancer-
435 inflammation that could be exploited utilising pharmaceutical control of this novel

436 HIF/COX/TNF mechanism. The zebrafish larvae is small enough to be fully oxygenated at
437 the 2-5dpf stages of this study (81). Further investigation of the HIF/COX/TNF axis in models
438 where hypoxia is a key hallmark of disease pathology is required to uncover the full
439 therapeutic relevance of this potentially important novel macrophage pathway.

440 In conclusion, we have identified a novel mechanism for macrophage *tnfa*
441 transcription via Hif-1α and cyclooxygenase that is conserved from zebrafish to humans,
442 highlighting a druggable mechanism to induce an M1-macrophage response. Importantly,
443 this axis links a microenvironmental cue, hypoxia, to a macrophage pro-inflammatory M1
444 cytokine, *tnfa* expression. We provide strong evidence to show that this response acts via
445 the cyclooxygenase/PGE2 arm of the arachidonic pathway. Due to the central roles of these
446 modulators in disease microenvironments we anticipate that this HIF/COX/TNF pathway
447 may have important implications in conditions such as inflammation, infection and cancer.
448
449 **References**

450 1. Benoit M, Desnues B, Mege J-L (2008) Infections Macrophage Polarization in
451 Bacterial Macrophage Polarization in Bacterial Infections. *J Immunol Ref J Immunol*
452 181:3733–3739.
453 2. Wiegertjes GF, Wentzel AS, Spaink HP, Elks PM, Fink IR (2016) Polarization of
454 immune responses in fish: The 'macrophages first' point of view. *Mol Immunol* 69.
455 doi:10.1016/j.molimm.2015.09.026.
456 3. Murray PJ, et al. (2014) Macrophage Activation and Polarization: Nomenclature and
457 Experimental Guidelines. *Immunity* 41(1):14–20.
458 4. Shapouri-Moghaddam A, et al. (2018) Macrophage plasticity, polarization, and
459 function in health and disease. *J Cell Physiol* 233(9):6425–6440.
460 5. Nizet V, Johnson RS (2009) Interdependence of hypoxic and innate immune
461 responses. *Nat Rev Immunol* 9(9):609–617.
462 6. Weiss G, Schaible UE (2015) Macrophage defense mechanisms against intracellular
463 bacteria. *Immunol Rev* 264(1):182–203.

464 7. Mortaz E, et al. (2015) Interaction of Pattern Recognition Receptors with
465 Mycobacterium Tuberculosis. *J Clin Immunol* 35(1). doi:10.1007/s10875-014-0103-7.
466 8. Huang Z, et al. (2015) Mycobacterium tuberculosis-induced polarization of human
467 macrophage orchestrates the formation and development of tuberculous granulomas
468 in vitro. *PLoS One* 10(6). doi:10.1371/journal.pone.0129744.
469 9. Qin Y, et al. (2015) Macrophage-Microglia Networks Drive M1 Microglia Polarization
470 After Mycobacterium Infection. *Inflammation* 38(4):1609–1616.
471 10. Hussain Bhat K, Mukhopadhyay S (2015) Macrophage takeover and the host-bacilli
472 interplay during tuberculosis. *Future Microbiol* 10(5):853–872.
473 11. Wang J, et al. (2015) Mycobacterium tuberculosis suppresses innate immunity by
474 coopting the host ubiquitin system. *Nat Immunol* 16(3):237–245.
475 12. Ehrt S, et al. (2001) Reprogramming of the macrophage transcriptome in response to
476 interferon-gamma and Mycobacterium tuberculosis: signaling roles of nitric oxide
477 synthase-2 and phagocyte oxidase. *J Exp Med* 194(8):1123–1140.
478 13. Roy S, et al. (2018) Transcriptional landscape of Mycobacterium tuberculosis infection
479 in macrophages. *Sci Rep* 8(1). doi:10.1038/s41598-018-24509-6.
480 14. Dorhoi A, Kaufmann SHE (2015) Versatile myeloid cell subsets contribute to
481 tuberculosis-associated inflammation. *Eur J Immunol* 45(8):2191–2202.
482 15. McClean CM, Tobin DM (2016) Macrophage form, function, and phenotype in
483 mycobacterial infection: Lessons from tuberculosis and other diseases. *Pathog Dis*
484 74(7). doi:10.1093/femspd/ftw068.
485 16. Wang N, Liang H, Zen K (2014) Molecular mechanisms that influence the
486 macrophage M1-M2 polarization balance. *Front Immunol* 5(NOV).
487 doi:10.3389/fimmu.2014.00614.
488 17. Cramer T, et al. (2003) HIF-1α is essential for myeloid cell-mediated inflammation.
489 *Cell* 112(5):645–657.
490 18. Peyssonnaux C, et al. (2007) Cutting edge: Essential role of hypoxia inducible factor-
491 1alpha in development of lipopolysaccharide-induced sepsis. *J Immunol*

178(12):7516–7519.

19. Kaidi A, Qualtrough D, Williams AC, Paraskeva C (2006) Direct transcriptional up-regulation of cyclooxygenase-2 by hypoxia-inducible factor (HIF)-1 promotes colorectal tumor cell survival and enhances HIF-1 transcriptional activity during hypoxia. *Cancer Res* 66(13):6683–6691.

20. Lee JJ, et al. (2010) Hypoxia activates the cyclooxygenase-2-prostaglandin E synthase axis. *Carcinogenesis* 31(3):427–434.

21. Zhao L, et al. (2012) Involvement of COX-2/PGE2signalling in hypoxia-induced angiogenic response in endothelial cells. *J Cell Mol Med* 16(8):1840–1855.

22. Norris PC, Reichart D, Dumlao DS, Glass CK, Dennis EA (2011) Specificity of eicosanoid production depends on the TLR-4-stimulated macrophage phenotype. *J Leukoc Biol* 90(3):563–574.

23. Gupta S, Maurya MR, Stephens DL, Dennis EA, Subramaniam S (2009) An integrated model of eicosanoid metabolism and signaling based on lipidomics flux analysis. *Biophys J* 96(11):4542–4551.

24. Harizi H (2013) The immunobiology of prostanoid receptor signaling in connecting innate and adaptive immunity. *Biomed Res Int* 2013. doi:10.1155/2013/683405.

25. Mancini AD, Di Battista JD (2011) The cardinal role of the phospholipase A(2)/cyclooxygenase-2/prostaglandin E synthase/prostaglandin E(2) (PCPP) axis in inflammostasis. *Inflamm Res* 60(12):1083–92.

26. Xing Y, et al. (2015) COX2 is involved in hypoxia-induced TNF-α expression in osteoblast. *Sci Rep* 5(1):10020.

27. Meijer AH (2016) Protection and pathology in TB: learning from the zebrafish model. *Semin Immunopathol* 38(2):261–273.

28. Henry KM, Loynes C a, Whyte MKB, Renshaw S a (2013) Zebrafish as a model for the study of neutrophil biology. *J Leukoc Biol* 94(4):633–42.

29. Elks PM, Renshaw SA, Meijer AH, Walmsley SR, van Eeden FJ (2015) Exploring the HIFs, buts and maybes of hypoxia signalling in disease: lessons from zebrafish

models. *Dis Model Mech* 8(11):1349–1360.

30. Loynes CA, et al. (2010) Pivotal Advance: Pharmacological manipulation of inflammation resolution during spontaneously resolving tissue neutrophilia in the zebrafish. *J Leukoc Biol* 87(2):203–212.

31. Nguyen-Chi M, et al. (2015) Identification of polarized macrophage subsets in zebrafish. *Elife* 4(JULY 2015). doi:10.7554/eLife.07288.

32. Marjoram L, et al. (2015) Epigenetic control of intestinal barrier function and inflammation in zebrafish. *Proc Natl Acad Sci U S A* 112(9):2770–5.

33. Ogryzko N, et al. (2018) Macrophage Il-1beta protects against mycobacterial infection downstream of Hif-1alpha in zebrafish. *BioRxiv* 1(2):2000–2000.

34. Nusslein-Volhard C DR (2002) *Zebrafish: A Practical Approach* (Oxford University Press, Oxford). 1st ed.

35. Bojarczuk A, et al. (2016) Cryptococcus neoformans Intracellular Proliferation and Capsule Size Determines Early Macrophage Control of Infection. *Sci Rep* 6(1):21489.

36. Hall C, Flores M V, Storm T, Crosier K, Crosier P (2007) The zebrafish lysozyme C promoter drives myeloid-specific expression in transgenic fish. *BMC Dev Biol* 7:42.

37. Santhakumar K, et al. (2012) A zebrafish model to study and therapeutically manipulate hypoxia signaling in tumorigenesis. *Cancer Res* 72(16):4017–4027.

38. Elks PM, Loynes CA, Renshaw SA (2011) *Measuring inflammatory cell migration in the zebrafish* doi:10.1007/978-1-61779-207-6_18.

39. van der Sar AM, Spaink HP, Zakrzewska A, Bitter W, Meijer AH (2009) Specificity of the zebrafish host transcriptome response to acute and chronic mycobacterial infection and the role of innate and adaptive immune components. *Mol Immunol* 46(11–12):2317–2332.

40. Cui C, et al. (2011) Infectious disease modeling and innate immune function in zebrafish embryos. *Methods Cell Biol* 105:273–308.

41. Benard EL, et al. (2012) Infection of zebrafish embryos with intracellular bacterial pathogens. *J Vis Exp* (61). doi:10.3791/37813781 [pii].

548 42. Elks PM, et al. (2013) PLOS Pathogens: Hypoxia Inducible Factor Signaling
549 Modulates Susceptibility to Mycobacterial Infection via a Nitric Oxide Dependent
550 Mechanism. *PLoS Pathog* 9(12):e1003789.
551 43. Elks PM, et al. (2014) Mycobacteria counteract a TLR-mediated nitrosative defense
552 mechanism in a zebrafish infection model. *PLoS One* 9(6).
553 doi:10.1371/journal.pone.0100928.
554 44. Elks PM, et al. (2011) Activation of hypoxia-inducible factor-1alpha (Hif-1alpha) delays
555 inflammation resolution by reducing neutrophil apoptosis and reverse migration in a
556 zebrafish inflammation model. *Blood* 118(3):712–722.
557 45. Barrett TD, et al. (2011) Pharmacological Characterization of 1-(5-Chloro-6-
558 (trifluoromethoxy)-1H-benzoimidazol-2-yl)-1H-pyrazole-4-carboxylic Acid (JNJ-
559 42041935), a Potent and Selective Hypoxia-Inducible Factor Prolyl Hydroxylase
560 Inhibitor. *Mol Pharmacol* 79(6):910–920.
561 46. Wu K, et al. (2016) Stabilization of HIF-1α by FG-4592 promotes functional recovery
562 and neural protection in experimental spinal cord injury. *Brain Res* 1632:19–26.
563 47. Feng Y, Renshaw S, Martin P (2012) Live imaging of tumor initiation in zebrafish
564 larvae reveals a trophic role for leukocyte-derived PGE2. *Curr Biol* 22(13):1253–1259.
565 48. Tobin DM, et al. (2010) The lta4h locus modulates susceptibility to mycobacterial
566 infection in zebrafish and humans. *Cell* 140(5):717–730.
567 49. Evans RJ, et al. (2017) Fungal derived 15-keto-prostaglandin E_2 activates host
568 peroxisome proliferator-activated receptor gamma (PPAR-γ) to promote C.
569 neoformans growth during infection. *bioRxiv*:113167.
570 50. Stoop EJ, et al. (2011) Zebrafish embryo screen for mycobacterial genes involved in
571 the initiation of granuloma formation reveals a newly identified ESX-1 component. *Dis*
572 *Model Mech* 4(4):526–536.
573 51. Dockrell DH, Lee M, Lynch DH, Read RC (2001) Immune-Mediated Phagocytosis and
574 Killing of *Streptococcus pneumoniae* Are Associated with Direct and Bystander
575 Macrophage Apoptosis. *J Infect Dis*. doi:10.1086/323084.

576 52. Ghezzi P, et al. (1991) Hypoxia increases production of interleukin-1 and tumor
577 necrosis factor by human mononuclear cells. *Cytokine*. doi:10.1016/1043-
578 4666(91)90015-6.
579 53. Tobin DM, et al. (2012) Host genotype-specific therapies can optimize the
580 inflammatory response to mycobacterial infections. *Cell* 148(3):434–446.
581 54. Van Der Vaart M, et al. (2014) The DNA damage-regulated autophagy modulator
582 DRAM1 links mycobacterial recognition via TLP-MYD88 to authophagic defense. *Cell*
583 *Host Microbe* 15(6):753–767.
584 55. Berod L, et al. (2014) MyD88 signalling in myeloid cells is sufficient to prevent chronic
585 mycobacterial infection. *Eur J Immunol* 44(5):1399–1409.
586 56. Basu J, Shin D-M, Jo E-K (2012) Mycobacterial signaling through toll-like receptors.
587 *Front Cell Infect Microbiol* 2. doi:10.3389/fcimb.2012.00145.
588 57. Elks PM, et al. (2011) Activation of hypoxia-inducible factor-1α (hif-1α) delays
589 inflammation resolution by reducing neutrophil apoptosis and reverse migration in a
590 zebrafish inflammation model. *Blood* 118(3). doi:10.1182/blood-2010-12-324186.
591 58. Chen IJ, et al. (2018) Targeting the 15-keto-PGE2-PTGR2 axis modulates systemic
592 inflammation and survival in experimental sepsis. *Free Radic Biol Med* 115:113–126.
593 59. Tai HH, Ensor CM, Tong M, Zhou H, Yan F (2002) Prostaglandin catabolizing
594 enzymes. *Prostaglandins Other Lipid Mediat* 68–69:483–493.
595 60. Ghosh S, Paul A, Sen E (2013) Tumor Necrosis Factor Alpha-Induced Hypoxia-
596 Inducible Factor 1α-β-Catenin Axis Regulates Major Histocompatibility Complex Class
597 I Gene Activation through Chromatin Remodeling. *Mol Cell Biol* 33(14):2718–31.
598 61. Charbonneau M, et al. (2007) Hypoxia-inducible factor mediates hypoxic and tumor
599 necrosis factor alpha-induced increases in tumor necrosis factor-alpha converting
600 enzyme/ADAM17 expression by synovial cells. *J Biol Chem* 282(46):33714–24.
601 62. Imtiyaz HZ, Simon MC (2010) Hypoxia-inducible factors as essential regulators of
602 inflammation. *Curr Top Microbiol Immunol* 345(1):105–120.
603 63. Sandau KB, Zhou J, Kietzmann T, Brüne B (2001) Regulation of the Hypoxia-

inducible Factor 1α by the Inflammatory Mediators Nitric Oxide and Tumor Necrosis Factor-α in Contrast to Desferroxamine and Phenylarsine Oxide. *J Biol Chem* 276(43):39805–39811.

64. Coggins KG, et al. (2002) Metabolism of PGE2by prostaglandin dehydrogenase is essential for remodeling the ductus arteriosus. *Nat Med* 8(2):91–92.

65. Ulrichs T, Kaufmann SH (2006) New insights into the function of granulomas in human tuberculosis. *J Pathol* 208(2):261–269.

66. Flynn JL, Chan J, Lin PL (2011) Macrophages and control of granulomatous inflammation in tuberculosis. *Mucosal Immunol* 4(3):271–278.

67. Via LE, et al. (2008) Tuberculous granulomas are hypoxic in guinea pigs, rabbits, and nonhuman primates. *Infect Immun* 76(6):2333–2340.

68. Orphanidou D, et al. (1996) Tumour necrosis factor, interleukin-1 and adenosine deaminase in tuberculous pleural effusion. *Respir Med* 90(2):95–98.

69. Benard EL, Rougeot J, Racz PI, Spaink HP, Meijer AH (2016) Transcriptomic Approaches in the Zebrafish Model for Tuberculosis—Insights Into Host- and Pathogen-specific Determinants of the Innate Immune Response. *Adv Genet* 95:217–251.

70. Flynn JL, et al. (1995) Tumor necrosis factor-alpha is required in the protective immune response against Mycobacterium tuberculosis in mice. *Immunity* 2(6):561–72.

71. Kindler V, Sappino AP, Grau GE, Piguet PF, Vassalli P (1989) The inducing role of tumor necrosis factor in the development of bactericidal granulomas during BCG infection. *Cell* 56(5):731–740.

72. Ormerod LP (2004) Tuberculosis and anti-TNF-alpha treatment. *Thorax* 59(11):921,2004.

73. Wallis RS. d, Broder MS., Wong JY., Hanson ME., Beenhouwer DO. (2004) Granulomatous infectious diseases associated with tumor necrosis factor antagonists. *Clin Infect Dis* 38(9):1261–1265.

632 74. Xie X, Li F, Chen J-W, Wang J (2014) Risk of tuberculosis infection in anti-TNF-α
633 biological therapy: From bench to bedside. *J Microbiol Immunol Infect* 47(4):268–274.
634 75. Clay H, Volkman HE, Ramakrishnan L (2008) Tumor necrosis factor signaling
635 mediates resistance to mycobacteria by inhibiting bacterial growth and macrophage
636 death. *Immunity* 29(2):283–294.
637 76. Duque-Correa MA, et al. (2014) Macrophage arginase-1 controls bacterial growth and
638 pathology in hypoxic tuberculosis granulomas. *Proc Natl Acad Sci* 111(38):E4024–
639 E4032.
640 77. Qualls JE, Murray PJ (2016) Immunometabolism within the tuberculosis granuloma:
641 amino acids, hypoxia, and cellular respiration. *Semin Immunopathol* 38(2):139–152.
642 78. Ajdukovic J (2016) HIF-1 - A big chapter in the cancer tale. *Exp Oncol* 38(1):9–12.
643 79. Greenhough A, et al. (2009) The COX-2/PGE2 pathway: key roles in the hallmarks of
644 cancer and adaptation to the tumour microenvironment. *Carcinogenesis* 30(3):377–
645 386.
646 80. Landskron G, De La Fuente M, Thuwajit P, Thuwajit C, Hermoso MA (2014) Chronic
647 inflammation and cytokines in the tumor microenvironment. *J Immunol Res* 2014.
648 doi:10.1155/2014/149185.
649 81. Oehlers SH, et al. (2015) Interception of host angiogenic signalling limits
650 mycobacterial growth. *Nature*. doi:10.1038/nature13967.
651

652 **Acknowledgements**

653 The authors would like to thank The Bateson Aquarium Team for fish care and the IICD
654 Technical Team for practical assistance (University of Sheffield). We gratefully thank, Michel
655 Bagnat (Duke University) for providing their *TgBAC(tnfa:GFP)pd1028* transgenic line,
656 Georges Lutfalla (Montpellier University) for providing the *Tg(tnfa:eGFP-F)ump5Tg* line,
657 Annemarie Meijer (University of Leiden) for M. marinum strains. We thank David Dockrell
658 (University of Edinburgh), Paul Collini (University of Sheffield) and Jon Kilby (University of
659 Sheffield) for help with hMDM experiments. Thanks to Alison Condliffe and Benjamin

660 Durham (University of Sheffield) for use of, and invaluable help with, their hypoxia hood. We
661 would like to thank Robert Evans (The Francis Crick, London) and Catherine Loynes
662 (University of Sheffield) for helpful discussions and advice on prostaglandin modulation.
663 Thanks to Simon Johnston, Hannah Isles and Stephen Renshaw (University of Sheffield) for
664 constructive comments on the manuscript.

665

666 **Funding**

667 AL and PME are funded by a Sir Henry Dale Fellowship jointly funded by the Wellcome
668 Trust and the Royal Society (Grant Number 105570/Z/14/Z) held by PME.

669

670 **Author Contributions**

671 Conceived and designed the experiments: PME, AL. Performed the experiments: PME, AL.
672 Analysed the data: PME, AL. Wrote the paper: PME.

673

674 **Figure Legends**

675

676 **Figure 1. Macrophage *tnfa:GFP* is upregulated by injury, Mm infection and Hif-1α**
677 **stabilisation**

678 (A) Fluorescent confocal micrographs of 3 days post fertilisation larvae with or without tailfin
679 wound (induced 16 hours previously) with example macrophages at the tailfin site. *tnfa*
680 expression was detected by GFP levels, in green, using the *TgBAC(tnfa:GFP)pd1028*
681 transgenic line. Macrophages are shown in red using a *Tg(mpeg1:mCherryCAAX)sh378*
682 line. The asterisk in the not wounded control indicates a neuromast that is fluorescent in all
683 channels as a marker of position.

684 (B) Fluorescent confocal micrographs of 1dpi Mm infected larvae, prior to granuloma
685 formation (left panels), and 4 dpi, early granuloma (right panels) stages of infection. *tnfa*
686 expression was detected by GFP levels, in green, using the *TgBAC(tnfa:GFP)pd1028*

687 transgenic line. Mm mCrimson is shown in the far-red (cyan) channel. Increased levels of
688 *tnfa:GFP* expression were detectable in cells associated with infection.
689 (C) Fluorescent confocal micrographs of 1 day post infection (dpi) caudal vein region of
690 infection. *tnfa* expression was detected by GFP levels, in green, using the
691 *TgBAC(tnfa:GFP)pd1028* transgenic line. Macrophages are shown in red using a
692 *Tg(mpeg1:mCherryCAAX)sh378* line. Mm Crimson is shown in the far-red channel (cyan,
693 right panels) with a PVP control (left panels). Without infection there is little detectable
694 *tnfa:GFP* expression, while infected and uninfected macrophages have higher levels of
695 *tnfa:GFP* in the Mm group. Dotted lines indicate the yolk extension of the larvae where there
696 is non-specific fluorescence.
697 (D) Fluorescent confocal micrographs of 2 days post fertilisation larvae in the caudal vein
698 region. *tnfa* expression was detected by GFP levels, in green, using the
699 *TgBAC(tnfa:GFP)pd1028* transgenic line. Macrophages are shown in red using a
700 *Tg(mpeg1:mCherryCAAX)sh378* line. Larvae were injected at the 1 cell stage with dominant
701 active (DA) Hif-1α or phenol red (PR) control.
702 (E) Fluorescent confocal micrographs of 2dpf zebrafish imaged around the caudal vein
703 region. *tnfa* expression was detected by GFP levels, in green, using the
704 *TgBAC(tnfa:GFP)pd1028* transgenic line. Larvae were injected at the 1 cell stage with
705 dominant negative (DN) or dominant active (DA) Hif-1α or phenol red (PR) control. Dotted
706 lines indicate the yolk extension of the larvae where there is non-specific fluorescence.
707 (F) Graph shows corrected fluorescence intensity levels of *tnfa:GFP*. Dominant active Hif-1α
708 (DA1, filled bar) had significantly increased *tnfa:GFP* levels compared to phenol red (PR)
709 and dominant negative Hif-1α (DN1) injected controls (white bars). Data shown are mean ±
710 SEM, n=66 cells from 12 embryos accumulated from 3 independent experiments and
711 corresponds to images in (E).
712 (G) Fluorescent confocal micrographs of 2dpf *TgBAC(tnfa:GFP)pd1028* transgenic larvae
713 treated with DMOG or DMSO control. Dotted lines indicate the yolk extension of the larvae

where there is non-specific fluorescence. Graph shows corrected fluorescence intensity levels of *tnfa:GFP* confocal z-stacks in larvae. DMOG treated larvae (filled bars) had significantly increased *tnfa:GFP* levels compared to DMSO controls (white bars). Data shown are mean ± SEM, n=24 cells from 6 embryos representative of 2 independent experiments.

(G) Fluorescent confocal micrographs of 2dpf *TgBAC(tnfa:GFP)pd1028* transgenic larvae treated with the PHD inhibitor JNJ-42041935 or a DMSO solvent control. Dotted lines indicate the yolk extension of the larvae where there is non-specific fluorescence. Graph shows corrected fluorescence intensity levels of *tnf-a:GFP* confocal z-stacks at 2dpf treated with JNJ-42041935 (filled bars) or DMSO controls (white bars). Data shown are mean ± SEM, n=48 cells from 8 embryos accumulated from 2 independent experiments.

(H) Fluorescent confocal micrographs of 2dpf *TgBAC(tnfa:GFP)pd1028* transgenic larvae treated with the PHD inhibitor FG4592 or a DMSO solvent control. Dotted lines indicate the yolk extension of the larvae where there is non-specific fluorescence. Graph shows corrected fluorescence intensity levels of *tnfa:GFP* confocal z-stacks in larvae at 2dpf treated with FG4592 (filled bars) or DMSO controls (white bars). Data shown are mean ± SEM, n=54 cells from 9 embryos accumulated from 3 independent experiments.

(I) Fluorescent confocal micrographs of 2dpf *TgBAC(tnfa:GFP)pd1028* transgenic larvae incubated in room normoxia or 5% oxygen (hypoxia) for 6 hours between 32-38hpf. Dotted lines indicate the yolk extension of the larvae where there is non-specific fluorescence. Graph shows corrected fluorescence intensity levels of *tnfa:GFP* confocal z-stacks in larvae at 2dpf incubated in 5% oxygen (filled bars) or normoxia controls (white bars). Data shown are mean ± SEM, n=72 cells from 12 embryos accumulated from 3 independent experiments.

Figure 2. Hif-1α-activated *tnfa:GFP* is cyclooxygenase dependent while injury and infection induced *tnfa:GFP* is cyclooxygenase independent

(A) Fluorescent confocal micrographs of 2dpf caudal vein region of larvae. *tnfa* expression was detected by GFP levels, in green, using the *TgBAC(tnfa:GFP)pd1028* transgenic line. Phenol red (PR) and dominant active Hif-1α (DA1) injected larvae were treated with DMSO, SC560 (Cox-1 inhibitor) and NS398 (Cox-2 inhibitor). Dotted lines indicate the yolk extension of the larvae where there is non-specific fluorescence.

(B) Corrected fluorescence intensity levels of *tnfa:GFP* confocal z-stacks in PR (white bars) and DA1 (filled bars) injected larvae at 2dpf treated with Cox inhibitors. Data shown are mean ± SEM, n=36 cells from 6 embryos representative of 3 independent experiments.

(C) Schematic of the arachidonic pathway indicating where stabilising Hif-1α upregulates *tnfa* via cyclooxygenase, an effect that is blocked using the Cox1/2 inhibitors SC560/NS398.

(D) Fluorescent confocal micrographs of 3 days post fertilisation larvae with or without tailfin wound (induced 16 hours previously) in phenol red (PR) or dominant active Hif-1α embryos. *tnfa* expression was detected by GFP levels, in green, using the *TgBAC(tnfα:GFP)pd1028* transgenic line. Embryos were treated with DMSO or NS398 (Cox-2 inhibitor).

(E) Corrected fluorescence intensity levels of *tnfa:GFP* confocal z-stacks in PR (white bars) and DA1 (filled bars) injected larvae at 2dpf treated with Cox inhibitors. Data shown are mean ± SEM, n=24 (in not wounded) or n=36 (in wounded) cells from 6 embryos accumulated from 2 independent experiments. Not-wounded fish had fewer macrophages at the tailfin site, hence the lower cell number in these groups.

(F) Fluorescent confocal micrographs of 1dpi caudal vein region of Mm Crimson infected larvae. *tnfa* expression was detected by GFP levels, in green, using the *TgBAC(tnfa:GFP)pd1028* transgenic line. Phenol red (PR) and dominant active Hif-1α (DA1) injected larvae were treated with DMSO, SC560 (Cox-1 inhibitor) and NS398 (Cox-2 inhibitor) and infected with Mm Crimson. Dotted lines indicate the yolk extension of the larvae where there is non-specific fluorescence.

(G) Corrected fluorescence intensity levels of *tnfa:GFP* confocal z-stacks in PR (white bars) and DA1 (filled bars) Mm Crimson infected larvae at 1dpi treated with Cox inhibitors. NB,

768 DMSO NoMm is a no Mm control taken from figure 2B for comparison with Mm infected data
769 (data is from the same experiment). Data shown are mean ± SEM, n=36 cells from 6
770 embryos representative of 3 independent experiments.
771 (H) Schematic showing that injury and infection upregulate *tnfa* independently of
772 cyclooxygenase, an effect that is not blocked by the Cox1/2 inhibitors SC560/NS398.
773
774 **Figure 3. Blocking 15-lipoxygenase or leukotriene B4 receptors does not abrogate**
775 **DA-Hif-1α-upregulation of *tnfa:GFP***
776 (A) Fluorescent confocal micrographs of 1dpi caudal vein region of Mm and PVP infected
777 larvae. *tnfa* expression was detected by GFP levels, in green, using the
778 *TgBAC(tnfa:GFP)pd1028* transgenic line. Phenol red (PR) and dominant active Hif-1α (DA1)
779 injected larvae were treated with DMSO or PD146176 (15-Lipoxygenase inhibitor). Non-
780 infected larvae are in the left panels (PVP) and Mm Crimson infected larvae are in the right
781 panels (Mm). Dotted lines indicate the yolk extension of the larvae where there is non-
782 specific fluorescence.
783 (B) Corrected fluorescence intensity levels of *tnfa:GFP* confocal z-stacks in uninfected
784 larvae (PVP, empty bars) and infected larvae (Mm, filled bars) at 1dpi of data shown in (A)
785 after treatment with DMSO or PD146176 (15-Lipoxygenase inhibitor). Data shown are mean
786 ± SEM, n=42 cells from 7 embryos accumulated from 3 independent experiments.
787 (C) Bacterial burden at 4dpi after injection of DA Hif-1α (DA1) and 24 hours of the 15-
788 lipoxygenase inhibitor PD146176, using DMSO as a negative solvent control. Data shown
789 are mean ± SEM, n=48-50 as accumulated from 3 independent experiments.
790 (D) Fluorescent confocal micrographs of 1dpi caudal vein region of Mm and PVP infected
791 larvae shown in A. *tnfa* expression was detected by GFP levels, in green, using the
792 *TgBAC(tnfa:GFP)pd1028* transgenic line. Phenol red (PR) and dominant active Hif-1α (DA1)
793 injected larvae were treated with DMSO or U75302/LY255283 (BLTR1/2 inhibitors). Non-
794 infected larvae are in the left panels (PVP) and Mm Crimson infected larvae are in the right

795 panels (Mm). Dotted lines indicate the yolk extension of the larvae where there is non-
796 specific fluorescence.
797 (E) Corrected fluorescence intensity levels of *tnfa:GFP* confocal z-stacks in uninfected
798 larvae (PVP, empty bars) and infected larvae (Mm, filled bars) at 1dpi of data shown in (D)
799 after treatment with DMSO or U75302/LY255283 (BLTR1/2 inhibitors). Data shown are
800 mean ± SEM, n=30 cells from 5 embryos accumulated from 2 independent experiments.
801 (F) Schematic of the arachidonic pathway indicating where stabilising Hif-1α upregulates
802 tnfa via cyclooxygenase, an effect that is not blocked using the 15-lipoxygenase inhibitor
803 PD146176 or BLTR1/2 inhibitors U75302/LY255283.
804
805 **Figure 4. Hif-1α-induced *tnfa:GFP* requires active prostaglandin E2**
806 (A) Fluorescent confocal micrographs of 1dpi caudal vein region of Mm. *tnfa* expression was
807 detected by GFP levels, in green, using the *TgBAC(tnfa:GFP)pd1028* transgenic line.
808 Phenol red (PR) and dominant active Hif-1α (DA1) injected larvae were treated with DMSO
809 or SC560 (Cox-1 inhibitor) in the presence or absence of endogenous prostaglandin E2
810 (PGE2). All larvae are PVP injected. Dotted lines indicate the yolk extension of the larvae
811 where there is non-specific fluorescence.
812 (B) Fluorescent confocal micrographs of 1dpi caudal vein region. *tnfa* expression was
813 detected by GFP levels, in green, using the *TgBAC(tnfa:GFP)pd1028* transgenic line.
814 Phenol red (PR) and dominant active Hif-1α (DA1) injected larvae were treated with DMSO
815 or NS398 (Cox-2 inhibitor) in the presence or absence of endogenous prostaglandin E2
816 (PGE2). All larvae are PVP injected. Dotted lines indicate the yolk extension of the larvae
817 where there is non-specific fluorescence.
818 (C) Corrected fluorescence intensity levels of *tnfa:GFP* confocal z-stacks in PVP injected
819 phenol red (PR, empty bars) and dominant active Hif-1α (DA1, filled bars) larvae at 1dpi of
820 data shown in (B) after treatment with DMSO/NS398/PGE2. Data shown are mean ± SEM,
821 n=54 cells from 9 embryos accumulated from 3 independent experiments.

(D) Corrected fluorescence intensity levels of *tnfa:GFP* confocal z-stacks in PVP injected phenol red (PR, empty bars) and dominant active Hif-1α (DA1, filled bars) larvae at 1dpi of data shown in (B) after treatment with DMSO/NS398/PGE2. Data shown are mean ± SEM, n=54 cells from 9 embryos accumulated from 3 independent experiments.

(E) Fluorescent confocal micrographs of 1dpi caudal vein region. *tnf-a* expression was detected by GFP levels, in green, using the *TgBAC(tnfa:GFP)pd1028* transgenic line. Phenol red (PR) and dominant active Hif-1α (DA1) injected larvae were treated with DMSO or NS398 (Cox-2 inhibitor) in the presence or absence of endogenous 15-keto prostaglandin E2 (15K). All larvae are PVP injected. Dotted lines indicate the yolk extension of the larvae where there is non-specific fluorescence.

(F) Corrected fluorescence intensity levels of *tnfa:GFP* confocal z-stacks in PVP injected phenol red (PR, empty bars) and dominant active Hif-1α (DA1, filled bars) larvae at 1dpi of data shown in (E) after treatment with DMSO/NS398/15-keto PGE2. Data shown are mean ± SEM, n=24 cells from 4 embryos accumulated from 2 independent experiments.

(G) Schematic of the arachidonic pathway indicating where blocking cyclooxygenase prevents Hif-1α upregulation of *tnfa*, an effect rescued by endogenous PGE2.

Figure 5. Hypoxia induces TNF in human MDMs in a COX-2 dependent manner

(A) TNF ELISA of human monocyte derived macrophages incubated in normoxia or 0.8% hypoxia with or without treatment with NS398. Data shown are mean ± SEM, n=5-8 biological repeats from 3-4 donors.

(B) TNF ELISA of human monocyte derived macrophages incubated in normoxia treated with FG4592 with or without treatment with NS398. Data shown are mean ± SEM, n=6 biological repeats from 3 donors.

Figure S1. Mm infection induced *tnfa:GFP* in macrophages in a second transgenic line.

Fluorescent confocal micrographs of 1dpi caudal vein region of infection. *tnfa* expression was detected by GFP levels, in green, using the *Tg(tnfa:eGFP-F)ump5Tg* transgenic line. Macrophages are shown in red using a *Tg(mpeg1:mCherry-F)ump2Tg* line. Mm Crimson is shown in the blue channel. Dotted lines indicate the yolk extension of the larvae where there is non-specific fluorescence.

Figure S2. 5% oxygen induces expression of the *phd3:GFP* hypoxia transgene.

Fluorescent micrographs of 48hpf *Tg(phd3:eGFP)i144* hypoxia reporter zebrafish after incubated in 6 hours of 5% oxygen from 32-38hpf, or normoxic controls.

Figure S3. DA-Hif-1α induced *il-1β:GFP* is not altered by Cox-1 inhibition and decreased by Cox-2 inhibition.

(A) Fluorescent confocal micrographs of 2dpf caudal vein region. *il-1β* expression was detected by GFP levels, in green, using the *TgBAC(il-1β:GFP)SH445* transgenic line. Macrophages are shown in red using a *Tg(mpeg1:mCherryCAAX)sh378* line. Without infection there is little detectable *il-1β:GFP* expression in phenol red (PR) controls, while DA-Hif-1α macrophages have higher levels of *il-1β:GFP* in the Mm group.

(B) Fluorescent confocal micrographs of 1dpi caudal vein region of PVP injected larvae. *il-1β* expression was detected by GFP levels. Phenol red (PR) and dominant active Hif-1α (DA1) injected larvae were treated with DMSO, SC560 (COX-1 inhibitor) and NS398 (COX-2 inhibitor).

(C) Corrected fluorescence intensity levels of *il-1β:GFP* confocal z-stacks in PVP injected larvae at 1dpi from (B). Data shown are mean ± SEM, n=36 cells from 6 embryos representative of 3 independent experiments.

Figure S4. Mm infection induced *tnfa:GFP* is not altered by Hif-1α stabilisation

(A) Fluorescent confocal micrographs of Mm Crimson infected 1dpi zebrafish imaged around the caudal vein region. *tnfa* expression was detected by GFP levels, in green, using the *TgBAC(tnfa:GFP)pd1028* transgenic line. Larvae were injected at the 1 cell stage with dominant negative (DN) or dominant active (DA) Hif-1α or phenol red (PR) control. Dotted lines indicate the yolk extension of the larvae where there is non-specific fluorescence.

(B) Graph shows corrected fluorescence intensity levels of *tnfa:GFP*. Dominant active Hif-1α (DA1, filled bar) showed no change in *tnfa:GFP* levels in the presence of Mm bacterial challenge compared to phenol red (PR) and dominant negative Hif-1α (DN1) injected controls (white bars). NB, PR NoMm is a no Mm control taken from figure 1A for comparison with Mm infected data, the data for which is from the same experiment as this one. Data shown are mean ± SEM, n=66 cells from 12 embryos accumulated from 3 independent experiments.

(C) Fluorescent confocal micrographs of 2dpf Mm infected *TgBAC(tnfa:GFP)pd1028* transgenic larvae treated with DMOG or DMSO control. Dotted lines indicate the yolk extension of the larvae where there is non-specific fluorescence.

(D) Graph shows corrected fluorescence intensity levels of *tnfa:GFP* confocal z-stacks in larvae. DMOG treated larvae (filled bars) had significantly increased *tnfa:GFP* levels compared to DMSO controls (white bars). Data shown are mean ± SEM, n=24 cells from 6 embryos representative of 2 independent experiments.

Figure S5. Cyclooxygenase inhibition does not block the protective effect of Hif-1α stabilisation in Mm infection.

(A) Bacterial burden of SC560 treated larvae at 4dpi after injection with phenol red (PR) or dominant active Hif-1α (DA1). Data shown are mean ± SEM, n=35 as accumulated from 3 independent experiments.

(B) Bacterial burden of NS398 treated larvae at 4dpi after injection with phenol red (PR) or dominant active Hif-1α (DA1). Data shown are mean ± SEM, n=35 as accumulated from 3 independent experiments.

(C) Bacterial burden of DMSO treated larvae at 4dpi after co-treatment with DMSO or DMOG. Data shown are mean ± SEM, n=33-36 as accumulated from 3 independent experiments.

(D) Bacterial burden of SC560 treated larvae at 4dpi after co-treatment with DMSO or DMOG. Data shown are mean ± SEM, n=33 as accumulated from 3 independent experiments.

(E) Bacterial burden of NS398 treated larvae at 4dpi after co-treatment with DMSO or DMOG. Data shown are mean ± SEM, n=33 as accumulated from 3 independent experiments.

Figure 1

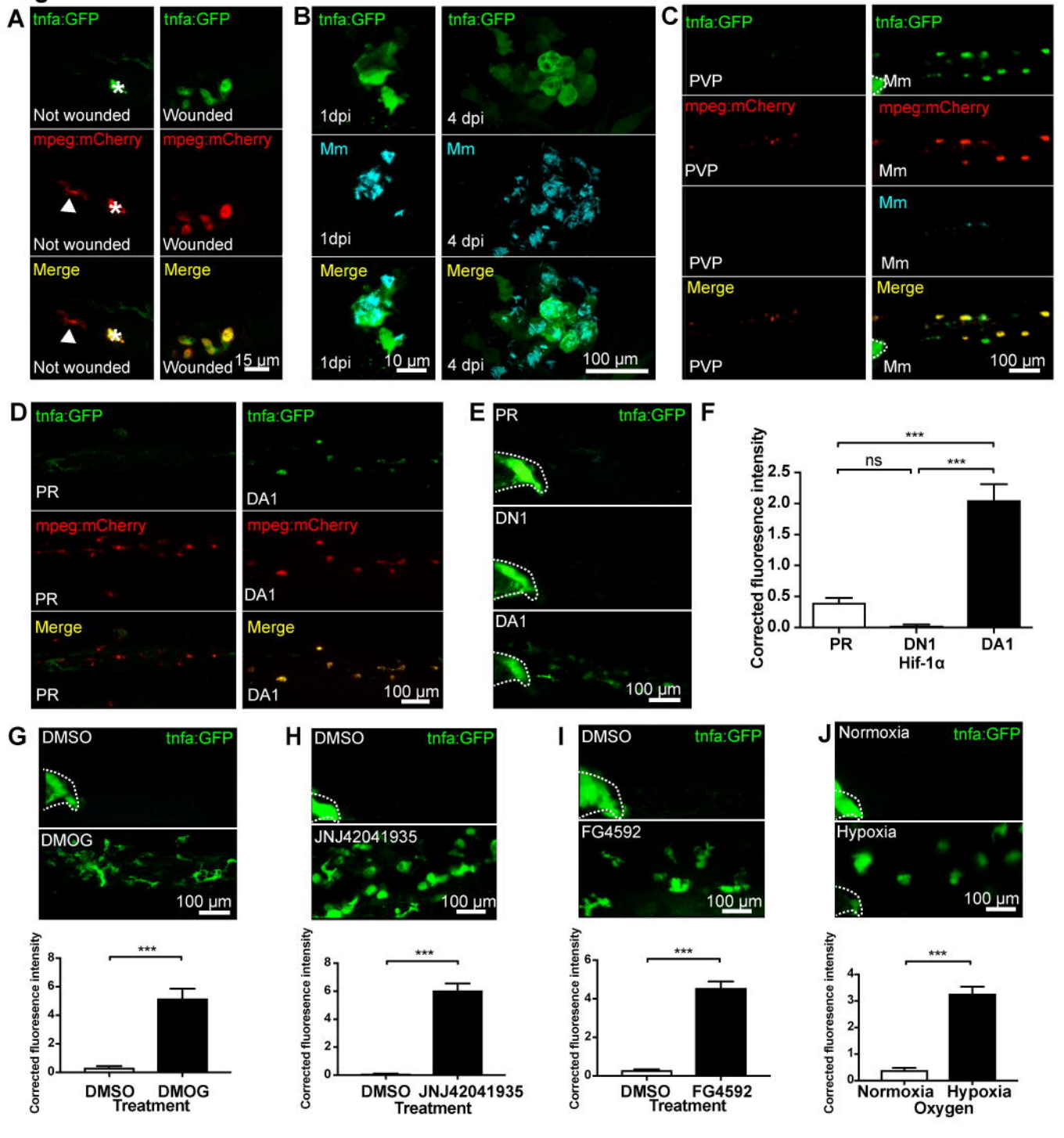
A
tnfa:GFP
Not wounded
Wounded
mpeg:mCherry
Merge
15 µm
B
1dpi
4 dpi
Mm
10 µm
100 µm
C
PVP
Mm
D
PR
DA1
E
DN1
F
Corrected fluoresence intensity
ns
***
Hif-1α
G
DMSO
DMOG
Treatment
H
JNJ42041935
I
FG4592
J
Normoxia
Hypoxia
Oxygen

Figure 2

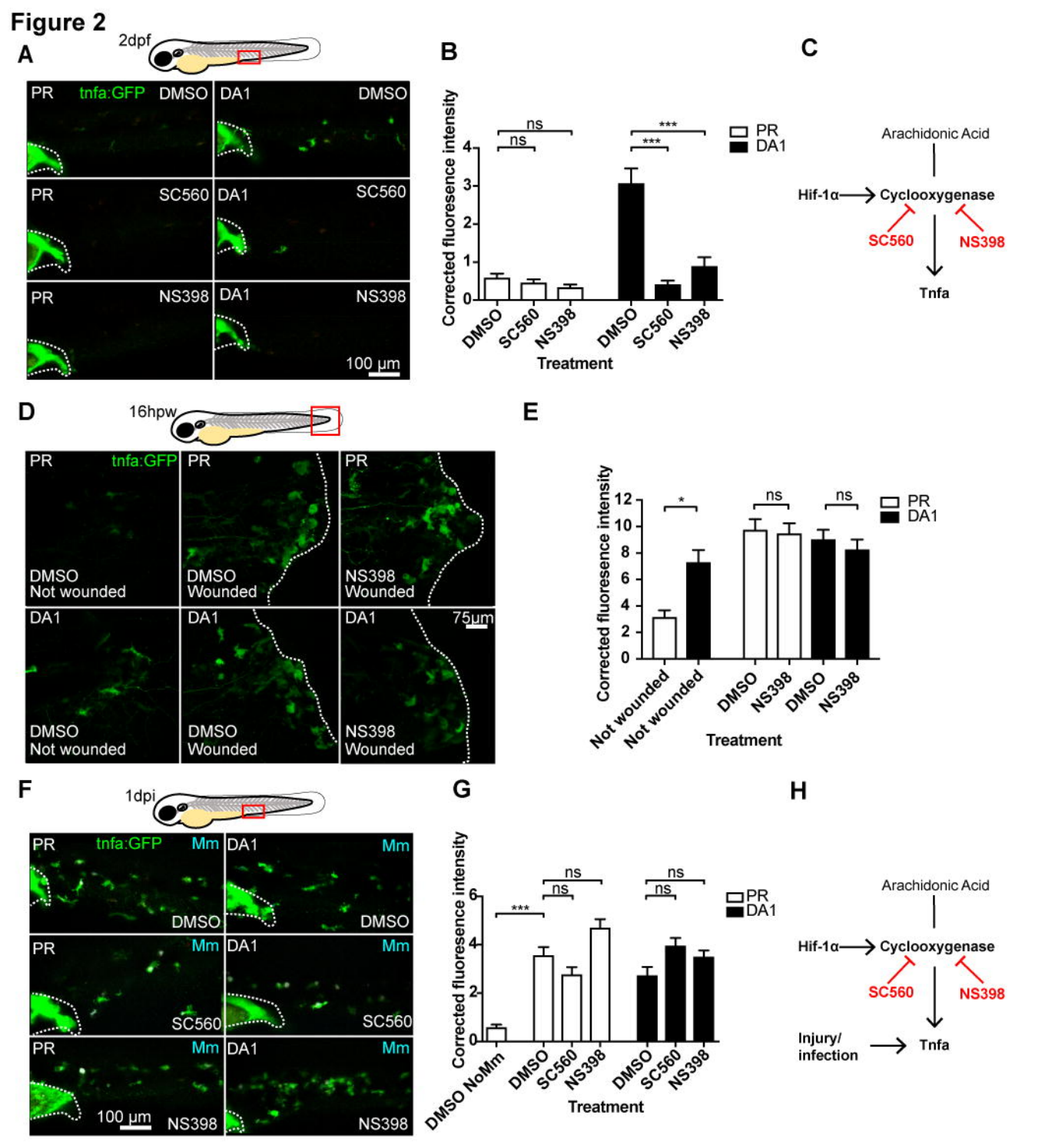
A
2dpf
PR tnfa:GFP DMSO
DA1 DMSO
PR SC560
DA1 SC560
PR NS398
DA1 NS398
100 µm
B
Corrected fluoresence intensity
ns
ns
***
***
PR
DA1
DMSO
SC560
NS398
DMSO
SC560
NS398
Treatment
C
Arachidonic Acid
Hif-1α
Cyclooxygenase
SC560
NS398
Tnfa
D
16hpw
PR tnfa:GFP
PR
PR
DMSO Not wounded
DMSO Wounded
NS398 Wounded
DA1
DA1
DA1
75µm
DMSO Not wounded
DMSO Wounded
NS398 Wounded
E
Corrected fluoresence intensity
*
ns
ns
PR
DA1
Not wounded
Not wounded
DMSO
NS398
DMSO
NS398
Treatment
F
1dpi
PR tnfa:GFP Mm
DA1 Mm
DMSO
DMSO
PR Mm
DA1 Mm
SC560
SC560
PR Mm
DA1 Mm
100 µm
NS398
NS398
G
Corrected fluoresence intensity
***
ns
ns
ns
ns
PR
DA1
DMSO NoMm
DMSO
SC560
NS398
DMSO
SC560
NS398
Treatment
H
Arachidonic Acid
Hif-1α
Cyclooxygenase
SC560
NS398
Injury/ infection
Tnfa

Figure 3

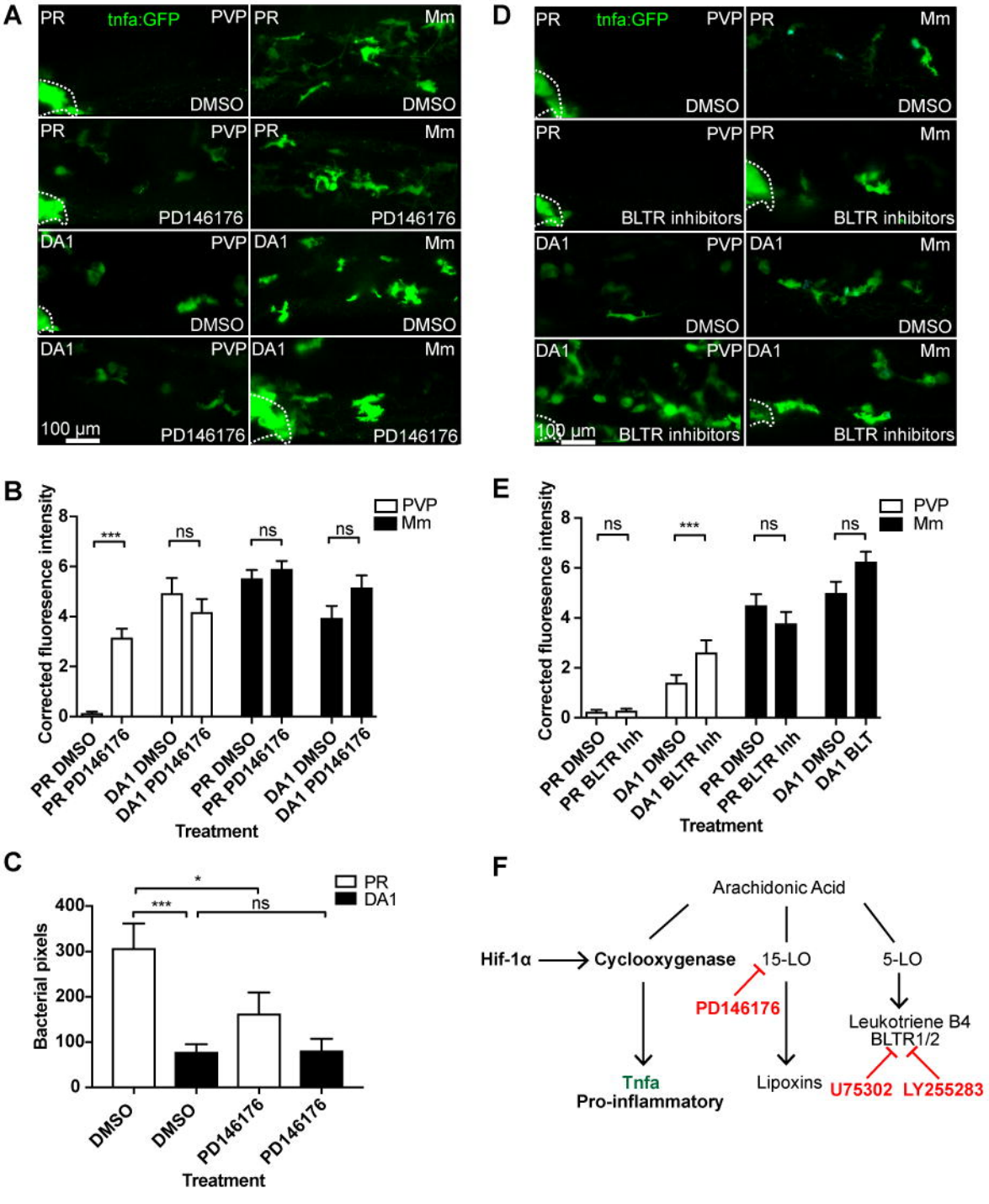
A
PR
tnfa:GFP
PVP
Mm
DMSO
PD146176
DA1
100 µm
D
BLTR inhibitors
B
Corrected fluoresence intensity
PVP
Mm
***
ns
PR DMSO
PR PD146176
DA1 DMSO
DA1 PD146176
Treatment
E
PR BLTR Inh
DA1 BLTR Inh
DA1 BLT
C
PR
DA1
Bacterial pixels
*
DMSO
F
Arachidonic Acid
Hif-1α
Cyclooxygenase
15-LO
5-LO
PD146176
Leukotriene B4
BLTR1/2
Tnfa
Pro-inflammatory
Lipoxins
U75302
LY255283

Figure 4

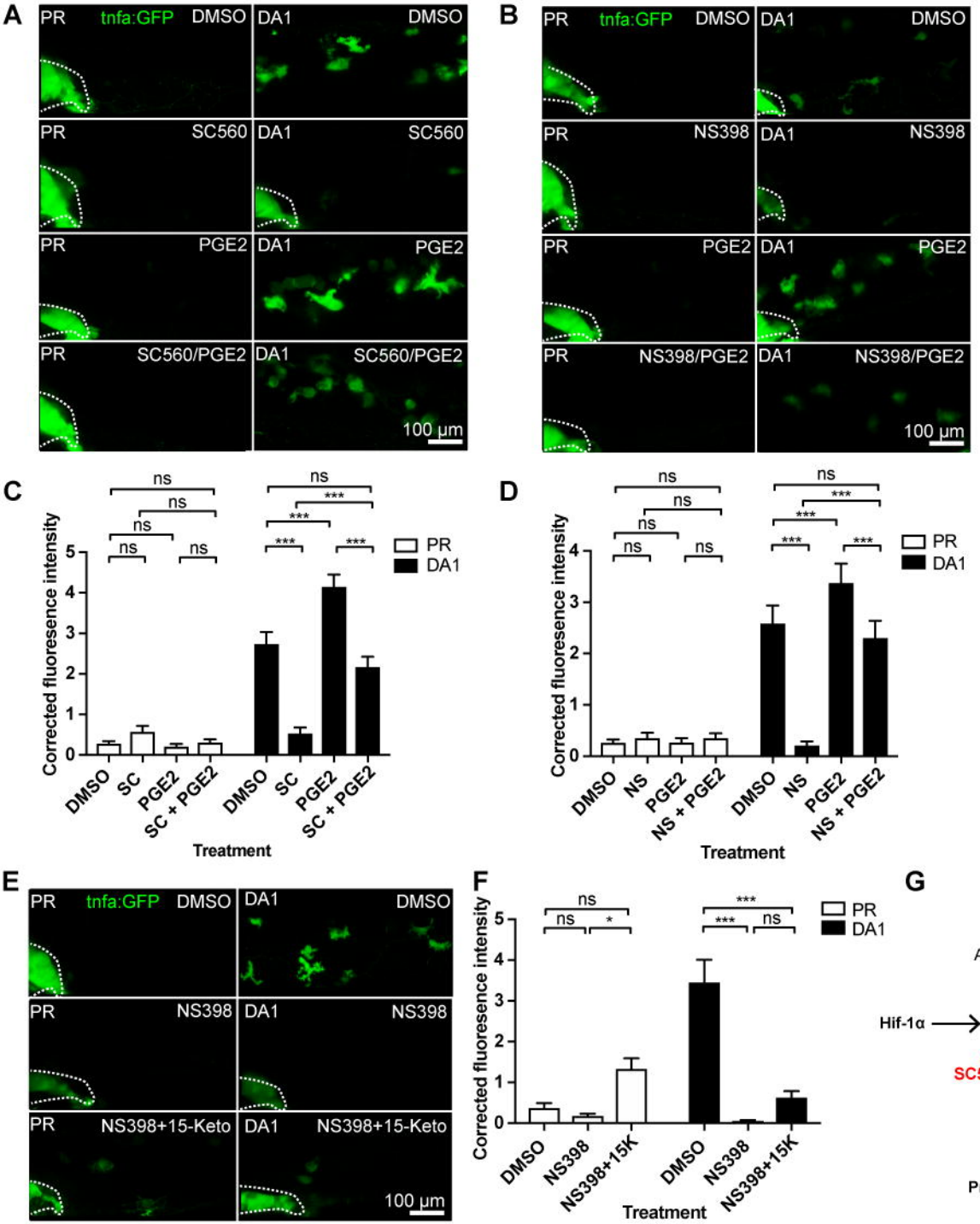
A
PR tnfa:GFP DMSO
DA1 DMSO
PR SC560
DA1 SC560
PR PGE2
DA1 PGE2
PR SC560/PGE2
DA1 SC560/PGE2
100 µm
B
PR tnfa:GFP DMSO
DA1 DMSO
PR NS398
DA1 NS398
PR PGE2
DA1 PGE2
PR NS398/PGE2
DA1 NS398/PGE2
100 µm
C
Corrected fluorescence intensity
PR
DA1
ns
***
DMSO
SC
PGE2
SC + PGE2
Treatment
D
Corrected fluorescence intensity
PR
DA1
ns
***
DMSO
NS
PGE2
NS + PGE2
Treatment
E
PR tnfa:GFP DMSO
DA1 DMSO
PR NS398
DA1 NS398
PR NS398+15-Keto
DA1 NS398+15-Keto
100 µm
F
Corrected fluorescence intensity
PR
DA1
ns
*
***
DMSO
NS398
NS398+15K
Treatment
G
Arachidonic Acid
Hif-1α
Cyclooxygenase
PGE2
SC560
NS398
Tnfa
Pro-inflammatory

Figure 5

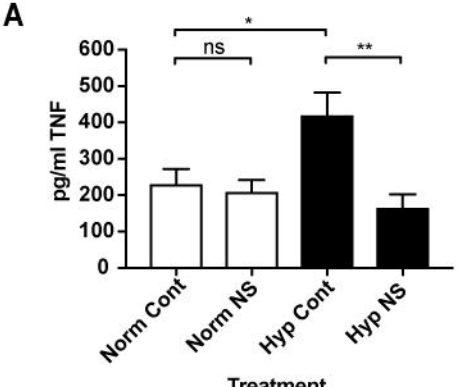
A
*
ns
**
600
500
400
300
200
100
0
pg/ml TNF
Norm Cont
Norm NS
Hyp Cont
Hyp NS
Treatment

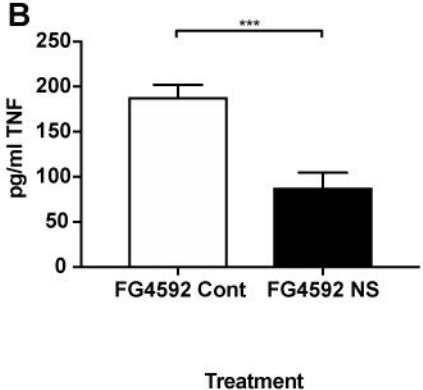
B
***
250
200
150
100
50
0
pg/ml TNF
FG4592 Cont
FG4592 NS
Treatment